Topological Superconductivity Mediated by Skyrmionic Magnons

Kristian Mæland and Asle Sudbø*
Center for Quantum Spintronics, Department of Physics, Norwegian University of Science and Technology, NO-7491 Trondheim, Norway

Topological superconductors are associated with the appearance of Majorana bound states, with promising applications in topologically protected quantum computing. In this Letter, we study a system where a skyrmion crystal is interfaced with a normal metal. Through interfacial exchange coupling, spin fluctuations in the skyrmion crystal mediate an effective electron-electron interaction in the normal metal. We study superconductivity within a weak-coupling approach and solve gap equations both close to the critical temperature and at zero temperature. Special features in the effective electron-electron interaction due to the noncolinearity of the magnetic ground state yield topological superconductivity at the interface.

Introduction. Quantum computation aims to solve problems of potentially great societal impact considerably faster than conventional computers. To achieve this, the intention is to utilize the quantum mechanical notions of superposition and entanglement. Quantum decoherence due to small perturbations is a major challenge for proposed realizations, introducing the need for error correction [1]. In topological quantum computers, the idea is to use braiding of anyons as logic gates. Computations based on this are topologically protected against small perturbations [2]. In this setting, topological superconductivity (TSC) offers the prospect of realizing Majorana bound states (MBSs), which are non-Abelian anyons. Braiding of MBSs is one of the most prominent propositions for topologically protected quantum computations [2–7].

There has been considerable interest in creating TSC at the interface between chiral magnets and conventional superconductors (SCs) [7–16]. The case of noncoplanar, skyrmion ground states in the chiral magnets has been given much attention, since MBSs can be localized at the centers of skyrmions [10] or bound states of skyrmions and vortices [11]. Bound states of skyrmions and superconducting vortices have been observed in Ref. [16]. Signatures of MBSs have been observed in a SC monolayer proximitized to magnetic islands [4], and at the ends of one-dimensional nanowire SCs [5]. Binding Majoranas to skyrmions is particularly interesting, since skyrmions can be moved by electric currents [10, 11, 17, 18]. To reach the topologically nontrivial regime, the theoretical proposals typically study a strong interaction between the spins in the magnet and the electrons in the SC [7–12].

Magnon-mediated superconductivity in heterostructures of colinear magnets and conductors has received a great deal of attention, often considering much weaker coupling across the interface [19–25]. All of these studies find topologically trivial SCs. Superconductivity mediated by spin fluctuations has been observed in a bilayer of bismuth and nickel [26].

In this Letter, we study magnon-mediated superconductivity in a normal metal (NM) due to spin fluctuations in skyrmion crystals (SkXs). Their noncolinearity leads to fundamentally new effects in the effective electron-electron interactions that give rise to TSC. We study superconductivity with a weak-coupling approach and solve both the linearized gap equation and the zero temperature gap equation. A bulk topological invariant is calculated to determine which parts of the superconducting phase diagram are topologically nontrivial.

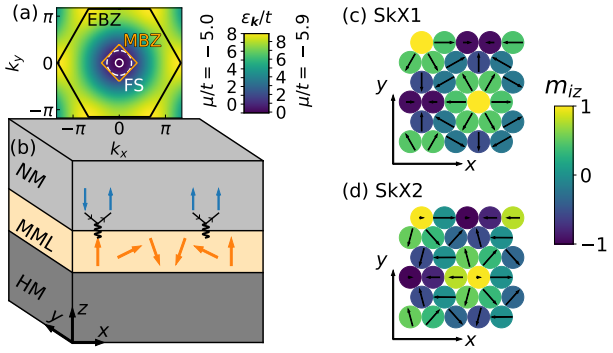

FIG. 1. (a) Plot of the electron energy $\epsilon_{\boldsymbol{k}}$ showing the electron first Brillouin zone (EBZ) in black, the magnetic first Brillouin zone (MBZ) in orange and the Fermi surface (FS) in white. Two choices of μ are shown, where the solid FS corresponds to $\mu/t = -5.9$ and the dashed FS corresponds to $\mu/t = -5.0$. (b) An illustration of the system under consideration. The itinerant electrons (blue arrows) in a normal metal (NM) are coupled to the spins (orange arrows) in a magnetic monolayer (MML). The MML is deposited on a heavy metal (HM) such that skyrmion crystal (SkX) ground states (GSs) are preferred. The (c) SkX1 and (d) SkX2 GSs are shown with periodic boundary conditions. Colors give the z component of the spins, m_{iz}, and arrows show their inplane component.

Model. The system is shown in Fig. 1(b). The insulating magnetic monolayer (MML) is modeled by a nearest-neighbor ferromagnetic exchange interaction of strength J, a Dzyaloshinskii-Moriya interaction (DMI) of strength D, a four-spin interaction of strength U, and an easy-axis anisotropy of strength K [27–29]. Motivated by Refs. [30, 31], we consider K to be a tunable parameter. Throughout, we set $\hbar = a = 1$, where a is the lattice constant. The role of the heavy metal (HM) is to provide the spin-orbit coupling necessary for DMI. In addition, hydridization [32] can lead to an unusually small nearest-neighbor exchange interaction so that the four-spin interaction is not negligible. Other than that, the HM has no effect on our model, which focuses on the two-dimensional (2D) interface between the NM and the MML. DMI prefers noncolinear magnetically ordered ground states (GSs). Among those, the four-spin interaction prefers

noncoplanar, dense SkXs [32]. The two classical GSs in the MML are shown in Fig. 1(c) and (d). SkX1 is the GS for $K < K_t$ and SkX2 is the GS for $K > K_t$, where $K_t/J \in (0.518, 0.519)$ as previously reported in Refs. [27, 28]. Note that the centers of the skyrmions in SkX2 are shifted compared to SkX1, giving SkX2 a lower symmetry [27]. These SkXs both feature 15 magnon bands, $\omega_{\boldsymbol{q}n}$, which we take as inputs in this Letter, $H_{\rm MML} = \sum_{\boldsymbol{q}\in{\rm MBZ},n} \omega_{\boldsymbol{q}n} b^\dagger_{\boldsymbol{q}n} b_{\boldsymbol{q}n}$. The quasimomentum $\boldsymbol{q}$ is restricted to the magnetic first Brillouin zone (MBZ) corresponding to the centered rectangular lattice set up by the SkX GSs [27, 28].

The NM at the interface is modeled by a hopping term with energy t and a controllable chemical potential, μ, which is diagonalized by a Fourier transform (FT) $c_{i\sigma} = \frac{1}{\sqrt{N}} \sum_{\boldsymbol{k}\in{\rm EBZ}} c_{\boldsymbol{k}\sigma} e^{i\boldsymbol{k}\cdot\boldsymbol{r}_i}$. The quasimomentum $\boldsymbol{k}$ is restricted to the electron first Brillouin zone (EBZ) corresponding to the triangular lattice, and N is the total number of lattice sites at the interface. $c_{i\sigma}$ annihilates an electron with spin σ and site index i, located at $\boldsymbol{r}_i$. This yields $H_{\rm NM} = \sum_{\boldsymbol{k}\in{\rm EBZ},\sigma} \epsilon_{\boldsymbol{k}} c^\dagger_{\boldsymbol{k}\sigma} c_{\boldsymbol{k}\sigma}$, with $\epsilon_{\boldsymbol{k}} = -\mu - 2t[\cos k_x + 2\cos(k_x/2)\cos(\sqrt{3}k_y/2)]$ shown in Fig. 1(a).

The interaction between electrons in the NM and localized spins in the MML is modeled as an interfacial exchange interaction [8–16, 19–26, 33], $H_{\rm em} = -2\bar{J}\sum_i \boldsymbol{c}^\dagger_i \boldsymbol{\sigma} \boldsymbol{c}_i \cdot \boldsymbol{S}_i$, where $\boldsymbol{c}_i = (c_{i\uparrow}, c_{i\downarrow})^T$, $\boldsymbol{\sigma}$ is a vector of the Pauli matrices, and $\boldsymbol{S}_i$ is the spin operator at site i. We treat this term as a perturbation to the NM, and focus on the magnon-mediated effective electron-electron interaction. Assuming $\bar{J} \ll t$ we keep the z axis as quantization axis for the electron spins in the NM. The spins in the MML are each quantized along the direction of the spin in the classical GS giving 15 separate quantization axes. Performing such rotations of the spins in the MML and applying the Holstein-Primakoff transformation, yields [29]

$$\begin{aligned} H_{\rm em} = &- \bar{J}\sqrt{2S}\sum_{i\sigma}[e^{-i\sigma\phi_i}(\cos\theta_i - n_\sigma)a_i c^\dagger_{i\sigma} c_{i,-\sigma} + {\rm H.c.}] \\ &+ \bar{J}\sqrt{2S}\sum_{i\sigma}(n_\sigma \sin\theta_i a_i c^\dagger_{i\sigma} c_{i\sigma} + {\rm H.c.}). \end{aligned} \tag{1}$$

Here, H.c. denotes Hermitian conjugate, $n_\uparrow = 1, n_\downarrow = -1$, a_i annihilates a magnon at site i, S is the spin quantum number in the MML, and θ_i, ϕ_i are the polar and azimuthal angles specifying the direction of the classical spin at site i. We have ignored terms that contain only two electron operators. Such renormalizations of the electron spectrum are higher order in perturbation theory than our weak-coupling treatment of the effective electron-electron interaction. Self-energy effects due to electron-magnon coupling could renormalize the electron spectrum. Given the existence of a magnon gap [27, 28], such effects are negligible close to the Fermi surface (FS) [34].

Compared to earlier studies of superconductivity induced by colinear spin structures, Eq. (1) features a fundamental difference. Namely, given that $\theta_i \neq \{0, \pi\}$, a magnon can be involved in both spin flip processes as well as processes where the z-component of the electron spin is not changed. We illustrate this in Fig. 1(b). When the spin in the magnet points in the z direction, the electron spin will always get a spin flip. When an itinerant electron interacts with a spin in the magnet with a nonzero inplane component, the electron spin need not change.

Effective interaction. As shown in Fig. 1(a), the MBZ is far smaller than the EBZ. Thus, Umklapp processes must be included when applying FTs to Eq. (1). The FT of the electron operators is modified to $c_{i\sigma} = \frac{1}{\sqrt{N}} \sum_{\boldsymbol{k}\in{\rm MBZ}} \sum_\nu c_{\boldsymbol{k}+\boldsymbol{Q}_\nu,\sigma} e^{i(\boldsymbol{k}+\boldsymbol{Q}_\nu)\cdot\boldsymbol{r}_i}$, where $\boldsymbol{Q}_\nu$ is a set of 15 reciprocal lattice vectors specified in Ref. [29]. If site i is located on sublattice r we have $a_i = \frac{1}{\sqrt{N'}} \sum_{\boldsymbol{q}\in{\rm MBZ}} a^{(r)}_{\boldsymbol{q}} e^{i\boldsymbol{q}\cdot\boldsymbol{r}_i}$, where N' is the number of magnetic unit cells. The magnon operators $a^{(r)}_{\boldsymbol{q}}$ are transformed to their diagonal basis $b_{\boldsymbol{q}n}$ through a paraunitary matrix $T_{\boldsymbol{q}}$ [27, 28, 35]. We obtain an effective electron-electron interaction mediated by the magnons in the SkXs by applying a Schrieffer-Wolff transformation [36]. Assuming oppositely directed momenta, we obtain [29]

$$H_{\rm ee} = \frac{1}{2}\sum_{\boldsymbol{k}\boldsymbol{k}'}^{\rm EBZ} \sum_{\substack{\sigma_1\sigma_2 \\ \sigma_3\sigma_4}} \bar{V}^{\sigma_1\sigma_2\sigma_3\sigma_4}_{\boldsymbol{k}\boldsymbol{k}'} c^\dagger_{\boldsymbol{k}'\sigma_1} c^\dagger_{-\boldsymbol{k}'\sigma_2} c_{-\boldsymbol{k}\sigma_3} c_{\boldsymbol{k}\sigma_4}, \tag{2}$$

where $\boldsymbol{k}' = \boldsymbol{k} + \boldsymbol{q} + \boldsymbol{Q}_\nu$. The coupling functions $\bar{V}^{\sigma_1\sigma_2\sigma_3\sigma_4}_{\boldsymbol{k}\boldsymbol{k}'}$ are of order $\bar{J}^2/t$ and contain linear combinations of magnon transformation coefficients divided by $\epsilon_{\boldsymbol{k}} - \epsilon_{\boldsymbol{k}'} \pm \omega_{\pm\boldsymbol{q},n}$. Detailed expressions are given in Ref. [29]. Due to the noncolinear spin structure, they are in general nonzero for all combinations of spin-indices. This is a crucial difference from colinear spin structures, where only a subset are nonzero [21–25]. This endows the superconducting order parameter with richer spin-texture than in the colinear case. While we treat Umklapp effects in the effective interaction, their effect on the NM energy dispersion are ignored. Hence, our results are valid when the FS is smaller than the MBZ, i.e. low filling $\mu/t \leq -5.0$, where such effects do not influence occupied states.

Superconductivity. We follow the generalized BCS theory outlined in Ref. [37] for unconventional SCs. Since all $\bar{V}^{\sigma_1\sigma_2\sigma_3\sigma_4}_{\boldsymbol{k}\boldsymbol{k}'}$ are nonzero in general, we can have coexistence of singlet SC gap, $\Delta^{O(s)}_{\boldsymbol{k}\uparrow\downarrow} = (\Delta_{\boldsymbol{k}\uparrow\downarrow} - \Delta_{\boldsymbol{k}\downarrow\uparrow})/2$, and all triplet gaps $\Delta^{E(s)}_{\boldsymbol{k}\uparrow\downarrow} = (\Delta_{\boldsymbol{k}\uparrow\downarrow} + \Delta_{\boldsymbol{k}\downarrow\uparrow})/2$, $\Delta_{\boldsymbol{k}\uparrow\uparrow}$, and $\Delta_{\boldsymbol{k}\downarrow\downarrow}$. This yields two distinct bands in the SC, $E_{\boldsymbol{k}\pm} = (\epsilon^2_{\boldsymbol{k}} + {\rm Tr}\,\hat{\Delta}_{\boldsymbol{k}}\hat{\Delta}^\dagger_{\boldsymbol{k}}/2 \pm \sqrt{A_{\boldsymbol{k}}}/2)^{1/2}$, with $(\hat{\Delta}_{\boldsymbol{k}})_{\sigma\sigma'} = \Delta_{\boldsymbol{k}\sigma\sigma'}$ and, in our case, $A_{\boldsymbol{k}}/16 = (\Delta^{E(s)}_{\boldsymbol{k}\uparrow\downarrow})^2(\Delta^{O(s)}_{\boldsymbol{k}\uparrow\downarrow})^2 - \Delta_{\boldsymbol{k}\uparrow\uparrow}\Delta_{\boldsymbol{k}\downarrow\downarrow}(\Delta^{O(s)}_{\boldsymbol{k}\uparrow\downarrow})^2$. A more general expression for $A_{\boldsymbol{k}}$ is given in Ref. [29].

The gap equation is [29]

$$\boldsymbol{\Delta}_{\boldsymbol{k}} = -\sum_{\boldsymbol{k}'} \mathcal{V}_{\boldsymbol{k}'\boldsymbol{k}} \sum_\eta \left(\frac{\boldsymbol{\Delta}_{\boldsymbol{k}'}}{2} + \eta \boldsymbol{B}_{\boldsymbol{k}'}\right)\chi_{\boldsymbol{k}'\eta}. \tag{3}$$

Here, $\boldsymbol{\Delta}_{\boldsymbol{k}} = (\Delta^{O(s)}_{\boldsymbol{k}\uparrow\downarrow}, \Delta_{\boldsymbol{k}\uparrow\uparrow}, \Delta_{\boldsymbol{k}\downarrow\downarrow}, \Delta^{E(s)}_{\boldsymbol{k}\uparrow\downarrow})^T$, $\boldsymbol{B}_{\boldsymbol{k}} = (B^{O(s)}_{\boldsymbol{k}\uparrow\downarrow}, B_{\boldsymbol{k}\uparrow\uparrow}, B_{\boldsymbol{k}\downarrow\downarrow}, B^{E(s)}_{\boldsymbol{k}\uparrow\downarrow})^T$, $B^\dagger_{\boldsymbol{k}\sigma_1\sigma_2} = \frac{1}{4\sqrt{A_{\boldsymbol{k}}}} \frac{\partial A_{\boldsymbol{k}}}{\partial \Delta_{\boldsymbol{k}\sigma_1\sigma_2}}$, and $\chi_{\boldsymbol{k}\eta} = \tanh(\beta E_{\boldsymbol{k}\eta}/2)/2E_{\boldsymbol{k}\eta}$. $\mathcal{V}_{\boldsymbol{k}'\boldsymbol{k}}$ is a matrix containing the 16 coupling functions [29].

For temperatures close to the critical temperature $T_{\rm c}$ we linearize the gap equation. Since $\chi_{\boldsymbol{k}'\eta}$ is peaked at the FS

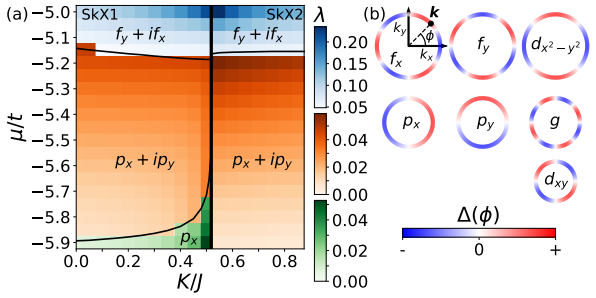

FIG. 2. (a) Phase diagram and dimensionless coupling λ in the superconducting state close to T_c. The vertical, black line shows the transition between SkX1 and SkX2 in the MML. The other black lines show the locations of the phase transitions with better resolution. In the green region, the unpolarized triplet gap $\Delta^{E(s)}_{\boldsymbol{k}\uparrow\downarrow}$ shows p_x-wave symmetry, while the other gaps are zero. In the orange and blue regions, the stated symmetry refers to the $\Delta_{\boldsymbol{k}\downarrow\downarrow}$ gap. The relevant gap symmetries are shown in (b). The parameters are $t/J = 1000$, $\bar{J}/J = 50$, $D/J = 2.16$, $U/J = 0.35$, and $S = 1$.

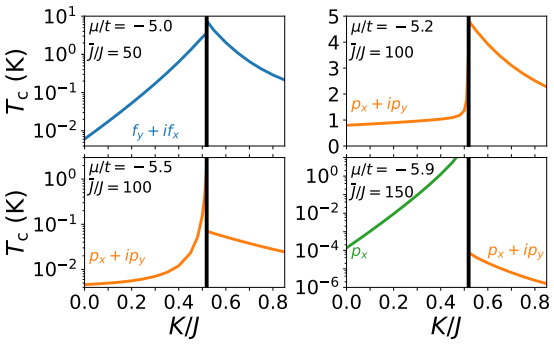

FIG. 3. Estimates of T_c as a function of the easy-axis anisotropy K in the MML for different chemical potentials μ. We have set an upper cutoff of 10 K since larger T_c means that $\lambda \ll 1$ is no longer valid. The parameters are $t/J = 1000$, $D/J = 2.16$, $U/J = 0.35$, and $S = 1$. In this figure only, $J = 1$ meV was set in order to find T_c in Kelvin.

for small T_c, we employ FS averages, keeping the angular dependence of $\mathcal{V}_{\boldsymbol{k}'\boldsymbol{k}}$, but ignoring any radial variation. The matrix elements are set to their value on the FS, for energies closer to the FS than the maximum magnon frequency ω_c, i.e. $|\epsilon_{\boldsymbol{k}}|, |\epsilon_{\boldsymbol{k}'}| < \omega_c$. Otherwise, the coupling functions are set to zero. The resulting gap equation is [29]

$$\lambda \boldsymbol{\Delta}(\phi) = -N_0 \langle \mathcal{V}(\phi', \phi) \boldsymbol{\Delta}(\phi') \rangle_{\mathrm{FS},\phi'}, \tag{4}$$

where N_0 is the density of states per spin on the FS, and ϕ is the angle $\boldsymbol{k}$ makes with the k_x axis. The dimensionless coupling constant λ can be used to estimate the critical temperature. Given $\lambda \ll 1$, $k_B T_c = (2e^\gamma/\pi)\omega_c e^{-1/\lambda}$, where γ is the Euler-Mascheroni constant [38]. We solve Eq. (4) as a matrix eigenvalue problem. Then, λ is the greatest eigenvalue and its corresponding eigenvectors give information about the structure of the gap [29].

Results for λ are given in Fig. 2(a). λ increases with μ, presumably because the FS becomes larger. λ also increases toward the phase transition between SkX1 and SkX2 in the MML, since the magnon gap decreases, giving stronger electron-electron interactions. Figure 2(a) also acts as a phase diagram showing the symmetry of the gaps. The proceeding symmetry classifications are illustrated in Fig. 2(b). In SkX1, for $K < K_t$, $\Delta^{E(s)}_{\boldsymbol{k}\uparrow\downarrow}$ decouples from the other gaps. In the green region, $\Delta^{E(s)}_{\boldsymbol{k}\uparrow\downarrow}$ has p_x-wave symmetry while the other gaps are zero. In the orange and blue regions, $\Delta^{E(s)}_{\boldsymbol{k}\uparrow\downarrow} = 0$. In the orange region, $\Delta_{\boldsymbol{k}\downarrow\downarrow}$ has $p_x + ip_y$-wave, i.e. chiral p-wave symmetry, $\Delta_{\boldsymbol{k}\uparrow\uparrow} = -\Delta^*_{\boldsymbol{k}\downarrow\downarrow}$ and $\Delta^{O(s)}_{\boldsymbol{k}\uparrow\downarrow}$ is a small d_{xy}-wave gap for low μ. For higher μ, $\Delta^{O(s)}_{\boldsymbol{k}\uparrow\downarrow}$ becomes g-wave. In the blue region, $\Delta_{\boldsymbol{k}\downarrow\downarrow}$ has $f_y + if_x$-wave, i.e. chiral f-wave symmetry, $\Delta_{\boldsymbol{k}\uparrow\uparrow} = -\Delta^*_{\boldsymbol{k}\downarrow\downarrow}$, while $\Delta^{O(s)}_{\boldsymbol{k}\uparrow\downarrow}$ shows $-d_{x^2-y^2}$-wave symmetry. The situation in SkX2 is similar, but all four gaps couple. While the other gap symmetries remain the same in the orange and blue regions, a comparatively small amplitude p_x-wave solution for $\Delta^{E(s)}_{\boldsymbol{k}\uparrow\downarrow}$ coexists.

Figure 3 shows estimates of T_c in Kelvin. Note from Fig. 2(a) that λ is too small in the orange and green regions to yield $T_c > 1$ mK when $\bar{J}/J = 50$. Here, $\lambda \sim (\bar{J}/t)^2$ and T_c depends exponentially on λ. Hence, an increase of $\bar{J}$ gives a major increase in T_c. We still keep $\bar{J} \ll t$, so that the coupling to the magnet can be viewed as a perturbation.

Zero temperature. To study the low-temperature behavior, we derive a gap equation at zero temperature, where $\chi_{\boldsymbol{k}\eta} = 1/2E_{\boldsymbol{k}\eta}$. Using FS averages yields [29]

$$\boldsymbol{\Delta}(\phi) = -N_0 \Bigg\langle \mathcal{V}(\phi', \phi) \sum_\eta \left(\frac{\boldsymbol{\Delta}(\phi')}{2} + \eta \boldsymbol{B}(\phi') \right) \times \operatorname{arsinh} \left[\frac{\sqrt{2}\omega_c}{\left(\operatorname{Tr} \hat{\Delta}(\phi') \hat{\Delta}^\dagger(\phi') + \eta \sqrt{A(\phi')} \right)^{1/2}} \right] \Bigg\rangle_{\mathrm{FS},\phi'}. \tag{5}$$

In the original BCS treatment of phonon-mediated superconductivity, $2\Delta(0)/k_B T_c = 2\pi e^{-\gamma}$ where $\Delta(0)$ is the amplitude of the gap at zero temperature [38]. We use this as the amplitude of an initial trial solution $\boldsymbol{\Delta}_0(\phi)$ with its structure around the FS guided by the solution close to T_c. Self-consistent iteration [29] is then used to obtain solutions of Eq. (5) satisfying a convergence criterion, typically 10^{-4} of the amplitude of the gap vector. The amplitude is defined as the largest absolute value of the real or imaginary parts of the four gap functions.

Figure 4 shows the resulting phase diagram at zero temperature. The black lines showing the phase transitions are wider, since there are regions where several symmetries can give solutions of the nonlinear Eq. (5) [29]. Let $\Delta(0)$ be the maximum of the lowest energy band on the FS, $\Delta(0) \equiv \max_{\mathrm{FS}} E_{\boldsymbol{k}-}$. This would be the largest gap found on the FS in an experiment. We see that $2\Delta(0)/k_B T_c$ is comparable to the BCS result in the p_x- and chiral p-wave phases, except that it drops to small values when approaching the phase transitions. In the chiral f-wave phases, $2\Delta(0)/k_B T_c$ is much smaller than the BCS result because $\operatorname{Tr} \hat{\Delta}_{\boldsymbol{k}} \hat{\Delta}^\dagger_{\boldsymbol{k}} \gtrsim \sqrt{A_{\boldsymbol{k}}}$ and

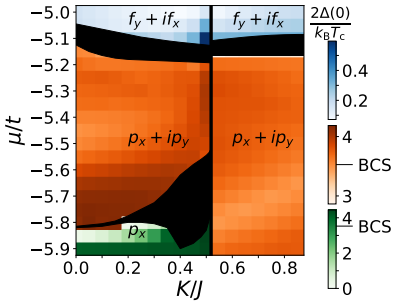

FIG. 4. Phase diagram at zero temperature showing $2\Delta(0)/k_{\mathrm{B}}T_{\mathrm{c}}$ in color. Black regions show where two or more symmetries lead to convergence. Where applicable, the BCS result $2\Delta(0)/k_{\mathrm{B}}T_{\mathrm{c}} = 2\pi e^{-\gamma}$ is shown on the colorbars. The parameters are $t/J = 1000$, $D/J = 2.16$, $U/J = 0.35$, and $S = 1$.

so $E_{\boldsymbol{k}-}$ is small. This is due to the unconventional nature of the SC. The value of $2\Delta(0)/k_{\mathrm{B}}T_{\mathrm{c}}$ has a very weak dependence on $\bar{J}$. We varied $\bar{J}$ when obtaining Fig. 4 to ensure that the expected amplitude at zero temperature was larger than $10^{-5}J$.

Topological superconductivity. The first requirement for (strong) TSC is a fully gapped bulk spectrum [6]. The chiral f-wave phases have a very small $E_{\boldsymbol{k}-}$, and we leave their topological classification as an open question. The p_x-wave phase is gapless and topologically trivial. In the chiral p-wave phases the bulk spectrum $E_{\boldsymbol{k}\eta}$ is fully gapped.

To determine if the SC state is topologically nontrivial, we proceed by computing a bulk topological invariant. We define a Bogoliubov-de Gennes (BdG) Hamiltonian where the gaps $\Delta_{\boldsymbol{k}\uparrow\downarrow}$ and $\Delta_{\boldsymbol{k}\downarrow\uparrow}$ are multiplied by $1-x$. Using the gap functions in the chiral p-wave phases we find that tuning x from 0 to 1 does not close the bulk gap [29]. Hence, the obtained SC is topologically equivalent to one where $\Delta_{\boldsymbol{k}\uparrow\downarrow} = \Delta_{\boldsymbol{k}\downarrow\uparrow} = 0$. For such a system, we can define two spin-decoupled BdG Hamiltonians $H_{\boldsymbol{k}\sigma} = \boldsymbol{d}_{\boldsymbol{k}\sigma}\cdot\boldsymbol{\sigma}$, where $\boldsymbol{d}_{\boldsymbol{k}\sigma} = (\mathrm{Re}\,\Delta_{\boldsymbol{k}\sigma\sigma}, -\mathrm{Im}\,\Delta_{\boldsymbol{k}\sigma\sigma}, \epsilon_{\boldsymbol{k}})$. The obtained SC states are time-reversal symmetric (TRS) [29, 37], and so the bulk topological invariant is defined as

$$\nu_{\mathbb{Z}_2} = \frac{1}{2}(N_\uparrow - N_\downarrow) \mod 2, \tag{6}$$

with $N_\sigma = (1/8\pi)\int_{\mathrm{EBZ}} d\boldsymbol{k}\epsilon_{ij}\hat{d}_{\boldsymbol{k}\sigma}\cdot(\partial_{k_i}\hat{d}_{\boldsymbol{k}\sigma}\times\partial_{k_j}\hat{d}_{\boldsymbol{k}\sigma})$, ϵ_{ij} the Levi-Civita tensor, $i,j\in\{x,y\}$, and $\hat{d}_{\boldsymbol{k}\sigma}$ a unit vector along $\boldsymbol{d}_{\boldsymbol{k}\sigma}$ [3]. Due to TRS, $N_\downarrow = -N_\uparrow$. Since the energy scale of $\epsilon_{\boldsymbol{k}}$ is much greater than the gaps $\Delta_{\boldsymbol{k}\sigma\sigma}$, the integrand is only nonzero close to the FS, where $\epsilon_{\boldsymbol{k}}$ is small. Hence, knowledge of the gaps close to the FS is sufficient to calculate the integral over the full EBZ. Using adaptive integration [28, 39], $N_\downarrow$ approaches 1 with increasing density of points. Therefore, $\nu_{\mathbb{Z}_2} = 1$, indicating a topologically nontrivial SC.

The chiral p-wave phases of our SC are TRS 2D topological SCs. In a finite geometry there will be two topologically protected, counterpropagating edge states which are Majorana fermions corresponding to each spin species [3]. Additionally, there will be MBSs in the core of vortices [2, 3].

TSC requires spinless or spin polarized Cooper pairs [3]. Previous studies of magnon-mediated superconductivity from colinear spin structures found only unpolarized Cooper pairs [22–25]. The noncolinearity of the SkXs admits the creation of polarized Cooper pairs, making TSC possible. In heterostructures of chiral magnets and conventional SCs, it is found that the noncoplanar nature of skyrmions is essential to get a bulk gap and strong TSC [6, 8, 9]. Unlike heterostructures involving conventional SCs, the pairing mechanism itself leads to TSC in the system we consider. From Eq. (1) it is clear that noncolinearity is sufficient to facilitate polarized Cooper pairs [40]. Whether noncolinear, coplanar states would result in TSC requires detailed solutions of the gap equation and is left as an open question.

Suggestions for materials. A SkX similar to SkX1 and SkX2 was observed in a MML of iron grown on top of the HM iridium [32]. To test our predictions, we suggest growing a NM which does not become a SC due to electron-phonon interactions, like copper, silver or gold [41], on top of the MML. Producing an interfacial exchange interaction strong enough to bring T_{c} to observable temperatures is a materials science challenge. The value of $\bar{J}$ is associated with an overlap integral, depending on the chosen materials and how the interface is grown. See Ref. [34] and references therein for a discussion of the value of $\bar{J}$. Note that while we require $\bar{J}/t \sim 0.1$ to get TSC with observable T_{c}, the studies of TSC in heterostructures of chiral magnets and conventional SCs often require $\bar{J} \sim t$ for the system to enter a topologically nontrivial state [7–12].

Conclusion. We have studied an interface between a normal metal and an insulating magnetic monolayer hosting skyrmion crystals. The noncolinearity of the magnetic ground state allowed more exotic electron-electron interactions mediated by magnons than colinear magnetic ground states. In large parts of the phase diagram, we found topological superconductivity, with possible applications in topological quantum computing.

Acknowledgments. We thank Jacob Benestad, Eirik Erlandsen, and Mathias Kläui for useful discussions. We acknowledge funding from the Research Council of Norway (RCN) through its Centres of Excellence funding scheme, Project No. 262633, "QuSpin," and RCN through Project No. 323766, "Equilibrium and out-of-equilibrium quantum phenomena in superconducting hybrids with antiferromagnets and topological insulators."

* Corresponding author: asle.sudbo@ntnu.no

[1] T. D. Ladd, F. Jelezko, R. Laflamme, Y. Nakamura, C. Monroe, and J. L. O'Brien, Quantum computers, Nature **464**, 45 (2010).
[2] C. Nayak, S. H. Simon, A. Stern, M. Freedman, and S. Das Sarma, Non-Abelian anyons and topological quantum computation, Rev. Mod. Phys. **80**, 1083 (2008).

[3] B. A. Bernevig and T. L. Hughes, *Topological Insulators and Topological Superconductors* (Princeton University Press, Princeton, NJ, 2013).

[4] G. C. Ménard, A. Mesaros, C. Brun, F. Debontridder, D. Roditchev, P. Simon, and T. Cren, Isolated pairs of Majorana zero modes in a disordered superconducting lead monolayer, Nat. Commun. **10**, 2587 (2019).

[5] M. Aghaee, A. Akkala, Z. Alam, R. Ali, A. Alcaraz Ramirez, M. Andrzejczuk, A. E. Antipov, M. Astafev, B. Bauer, J. Becker, *et al.*, InAs-Al Hybrid Devices Passing the Topological Gap Protocol, arXiv:2207.02472 (2022).

[6] M. Sato and Y. Ando, Topological superconductors: a review, Rep. Prog. Phys. **80**, 076501 (2017).

[7] A. O. Zlotnikov, M. S. Shustin, and A. D. Fedoseev, Aspects of Topological Superconductivity in 2D Systems: Noncollinear Magnetism, Skyrmions, and Higher-order Topology, J. Supercond. Nov. Magn. **34**, 3053 (2021).

[8] S. Nakosai, Y. Tanaka, and N. Nagaosa, Two-dimensional p-wave superconducting states with magnetic moments on a conventional s-wave superconductor, Phys. Rev. B **88**, 180503(R) (2013).

[9] W. Chen and A. P. Schnyder, Majorana edge states in superconductor-noncollinear magnet interfaces, Phys. Rev. B **92**, 214502 (2015).

[10] G. Yang, P. Stano, J. Klinovaja, and D. Loss, Majorana bound states in magnetic skyrmions, Phys. Rev. B **93**, 224505 (2016).

[11] S. Rex, I. V. Gornyi, and A. D. Mirlin, Majorana bound states in magnetic skyrmions imposed onto a superconductor, Phys. Rev. B **100**, 064504 (2019).

[12] S. A. Díaz, J. Klinovaja, D. Loss, and S. Hoffman, Majorana bound states induced by antiferromagnetic skyrmion textures, Phys. Rev. B **104**, 214501 (2021).

[13] N. Mohanta, S. Okamoto, and E. Dagotto, Skyrmion control of Majorana states in planar Josephson junctions, Commun. Phys. **4**, 163 (2021).

[14] M. Garnier, A. Mesaros, and P. Simon, Topological superconductivity with deformable magnetic skyrmions, Commun. Phys. **2**, 126 (2019).

[15] E. Mascot, J. Bedow, M. Graham, S. Rachel, and D. K. Morr, Topological superconductivity in skyrmion lattices, npj Quantum Mater. **6**, 6 (2021).

[16] A. P. Petrović, M. Raju, X. Y. Tee, A. Louat, I. Maggio-Aprile, R. M. Menezes, M. J. Wyszyński, N. K. Duong, M. Reznikov, C. Renner, M. V. Milošević, and C. Panagopoulos, Skyrmion-(Anti)Vortex Coupling in a Chiral Magnet-Superconductor Heterostructure, Phys. Rev. Lett. **126**, 117205 (2021).

[17] N. Nagaosa and Y. Tokura, Topological properties and dynamics of magnetic skyrmions, Nat. Nanotechnol. **8**, 899 (2013).

[18] G. Finocchio, F. Büttner, R. Tomasello, M. Carpentieri, and M. Kläui, Magnetic skyrmions: from fundamental to applications, J. Phys. D: Appl. Phys. **49**, 423001 (2016).

[19] M. Kargarian, D. K. Efimkin, and V. Galitski, Amperean Pairing at the Surface of Topological Insulators, Phys. Rev. Lett. **117**, 076806 (2016).

[20] H. G. Hugdal, S. Rex, F. S. Nogueira, and A. Sudbø, Magnon-induced superconductivity in a topological insulator coupled to ferromagnetic and antiferromagnetic insulators, Phys. Rev. B **97**, 195438 (2018).

[21] E. Erlandsen, A. Brataas, and A. Sudbø, Magnon-mediated superconductivity on the surface of a topological insulator, Phys. Rev. B **101**, 094503 (2020).

[22] N. Rohling, E. L. Fjærbu, and A. Brataas, Superconductivity induced by interfacial coupling to magnons, Phys. Rev. B **97**, 115401 (2018).

[23] E. L. Fjærbu, N. Rohling, and A. Brataas, Superconductivity at metal-antiferromagnetic insulator interfaces, Phys. Rev. B **100**, 125432 (2019).

[24] E. Erlandsen, A. Kamra, A. Brataas, and A. Sudbø, Enhancement of superconductivity mediated by antiferromagnetic squeezed magnons, Phys. Rev. B **100**, 100503(R) (2019).

[25] E. Thingstad, E. Erlandsen, and A. Sudbø, Eliashberg study of superconductivity induced by interfacial coupling to antiferromagnets, Phys. Rev. B **104**, 014508 (2021).

[26] X. Gong, M. Kargarian, A. Stern, D. Yue, H. Zhou, X. Jin, V. M. Galitski, V. M. Yakovenko, and J. Xia, Time-reversal symmetry-breaking superconductivity in epitaxial bismuth/nickel bilayers, Sci. Adv. **3**, e1602579 (2017).

[27] K. Mæland and A. Sudbø, Quantum fluctuations in the order parameter of quantum skyrmion crystals, Phys. Rev. B **105**, 224416 (2022).

[28] K. Mæland and A. Sudbø, Quantum topological phase transitions in skyrmion crystals, Phys. Rev. Res. **4**, L032025 (2022).

[29] See Supplemental Material at [URL will be inserted by publisher] for (i) the model for the magnetic monolayer, (ii) a derivation of the effective electron-electron interaction, (iii) derivations of the gap equations, (iv) plots of the gap functions, and (v) details of the calculation of the bulk topological invariant, which includes Refs. [42–46].

[30] R. Albaridy, A. Manchon, and U. Schwingenschlögl, Tunable magnetic anisotropy in Cr–trihalide Janus monolayers, J. Phys.: Condens. Matter **32**, 355702 (2020).

[31] L. Webster and J.-A. Yan, Strain-tunable magnetic anisotropy in monolayer $CrCl_3$, $CrBr_3$, and CrI_3, Phys. Rev. B **98**, 144411 (2018).

[32] S. Heinze, K. von Bergmann, M. Menzel, J. Brede, A. Kubetzka, R. Wiesendanger, G. Bihlmayer, and S. Blügel, Spontaneous atomic-scale magnetic skyrmion lattice in two dimensions, Nat. Phys. **7**, 713 (2011).

[33] Y. Kajiwara, K. Harii, S. Takahashi, J. Ohe, K. Uchida, M. Mizuguchi, H. Umezawa, H. Kawai, K. Ando, K. Takanashi, S. Maekawa, and E. Saitoh, Transmission of electrical signals by spin-wave interconversion in a magnetic insulator, Nature **464**, 262 (2010).

[34] K. Mæland, H. I. Røst, J. W. Wells, and A. Sudbø, Electron-magnon coupling and quasiparticle lifetimes on the surface of a topological insulator, Phys. Rev. B **104**, 125125 (2021).

[35] J. H. P. Colpa, Diagonalization of the quadratic boson Hamiltonian, Physica **93A**, 327 (1978).

[36] J. R. Schrieffer and P. A. Wolff, Relation between the Anderson and Kondo Hamiltonians, Phys. Rev. **149**, 491 (1966).

[37] M. Sigrist and K. Ueda, Phenomenological theory of unconventional superconductivity, Rev. Mod. Phys. **63**, 239 (1991).

[38] K. Fossheim and A. Sudbø, *Superconductivity: Physics and Applications* (Wiley, Chichester, England, 2004).

[39] S. E. Mousavi, J. E. Pask, and N. Sukumar, Efficient adaptive integration of functions with sharp gradients and cusps in n-dimensional parallelepipeds, Int. J. Numer. Methods Eng. **91**, 343 (2012).

[40] J. Benestad, Electron-magnon coupling and magnon-induced superconductivity in hybrid structures of metals and magnets with non-collinear ground states, Master's thesis, Norwegian University of Science and Technology (2022).

[41] C. Kittel, *Introduction to Solid State Physics*, 8th ed. (Wiley, New York, 2005).

[42] A. H. MacDonald, S. M. Girvin, and D. Yoshioka, t/U expansion for the Hubbard model, Phys. Rev. B **37**, 9753 (1988).

[43] B. Göbel, I. Mertig, and O. A. Tretiakov, Beyond skyrmions: Review and perspectives of alternative magnetic quasiparticles,

Phys. Rep. **895**, 1 (2021).

[44] J. T. Haraldsen and R. S. Fishman, Spin rotation technique for non-collinear magnetic systems: application to the generalized Villain model, J. Phys.: Condens. Matter **21**, 216001 (2009).

[45] F. J. dos Santos, M. dos Santos Dias, F. S. M. Guimarães, J. Bouaziz, and S. Lounis, Spin-resolved inelastic electron scattering by spin waves in noncollinear magnets, Phys. Rev. B **97**, 024431 (2018).

[46] P. Laurell and G. A. Fiete, Topological Magnon Bands and Unconventional Superconductivity in Pyrochlore Iridate Thin Films, Phys. Rev. Lett. **118**, 177201 (2017).